Received August 6, 2020, accepted August 28, 2020, date of publication September 1, 2020, date of current version September 15, 2020.

Digital Object Identifier 10.1109/ACCESS.2020.3020793

Crosspoint Localization of Spiral and Girth Welds of Spiral Steel Pipelines

JIAN LI, MINGZE LI, XINJING HUANG, FENG HAO, XIAOBO RUI, AND YU ZHANG

State Key Laboratory of Precision Measuring Technology and Instruments, Tianjin University, Tianjin 300072, China
Binhai International Advanced Structural Integrity Research Centre, Tianjin 300072, China

Corresponding author: Xinjing Huang (huangxinjing@tju.edu.cn)

This work was supported in part by the National Key Research and Development Project of China under Grant 2016YFC0802103, in part by the National Natural Science Foundation of China under Grant 61773283 and Grant 51604192, and in part by the Project funded by the China Postdoctoral Science Foundation under Grant 2018M630271.

ABSTRACT Crosspoint of spiral and girth welds of spiral steel pipelines transporting high-pressure oil and gas is easy to crack due to welding defects and corrosion, so routine excavation and careful inspection are required. In order to reduce the workload and cost of excavation, it is necessary to determine the crosspoint's angular position on the girth weld. This article proposes a low-cost and high-efficiency method for locating the spiral-girth weld crosspoint based on the inner Spherical Detector (SD). Theoretical analysis and experiments demonstrate that the magnetometer with a smaller lift-off could detect more noticeable magnetic valley of the spiral welds at the pipe bottom, so a smaller SD should be used; the spiral direction can be determined by the phase difference of the dual-channel magnetic signals, when dual magnetometers are symmetrically fixed about the median vertical plane on the rotation axis of the SD. When the girth weld, at least one spiral weld and the spiral direction are detected and determined, the crosspoint's angular position can be calculated. The maximum localization error of the crosspoint is less than 30° and the average error is less than 20°, that is, no more than one hour's angle, whose accuracy is sufficient for excavation and maintenance in the field, because it will reduce the amount of excavation by nearly half.

INDEX TERMS Spiral pipelines, welds, magnetic field, spherical detector.

I. INTRODUCTION

Transportation of oil and gas by pipelines has the advantages of low cost, high efficiency and high safety. Rapid development of the oil and gas transportation industry around the world has led to a huge increase in the number of pipelines. Oil and gas pipelines mainly include seamless steel pipe, straight welded steel pipe and spiral steel pipe [1]. Among them, seamless steel pipe has the highest strength and the strongest pressure bearing capacity, but with the increase of size, the cost increases rapidly. Although the manufacturing cost of straight welded steel pipe is low, its strength is very low, and it cannot operate stably under high pressure environment. Spiral steel pipe has lower cost and larger size than that of seamless steel pipe. In 2016 [1], China has upgraded the steel grade of gas transmission pipeline from X52 to X80, increased the pressure of gas transmission pipeline from 6.3MPa to 12MPa, and the transmission capacity of single pipeline has reached 30 billion m^3/a, and the gas explosion test proved that the strength of spiral welded pipe has higher strength than that of straight welded steel pipe [2]–[4]. Therefore, spiral steel pipe occupies a large share in oil and gas pipeline [5], [6]. A spiral pipeline is made by welding many sections of spiral pipes, so there are crosspoints of spiral and girth welds between adjacent sections. One section in a field spiral pipeline has two spiral-girth weld crosspoints, which are the spiral starts at the inlet and the outlet. Strength at the crosspoint is much lower than that at other parts of a spiral pipeline, and cracking here is easier to occur [2], [7]–[10]. It is required to excavate the soil outside the buried pipeline from a suitable direction, and expose the spiral-girth weld crosspoint for careful inspection. In order to reduce the workload and cost of excavation, it is necessary to determine the angular position of the crosspoint on the girth weld.

Currently, there are many techniques suitable for detecting and locating weld defects in pipelines, which can be divided into the following four categories: radiographic, ultrasonic, eddy current based and magnetic. Radiographic inspection

The associate editor coordinating the review of this manuscript and approving it for publication was Manuel Rosa-Zurera.

uses the intensity of the radiation passing through the spiral weld to detect whether the weld has cracks [11], [12]. Passive radio frequency identification (RFID) tag antenna is also deployed to exchange information to form a structural health monitoring system because of their passive, wireless, low cost and simple, compact size [13]. However, tens of thousands of antennas have to be deployed to cover all the spiral welds in the whole field pipeline. Ultrasonic inspection is to detect pipeline welds and defects by measuring the change of ultrasonic velocity in materials [14], [15]. It has a deeper penetration depth than radiographic inspection technology, but usually needs to apply coupling agent on the surface, and it is not suitable for the detection of rough surface. Eddy current inspection is based on electromagnetic induction, and uses the secondary eddy current generated by the pipe wall to detect pipeline defects and weld seams [16]–[19]. However, due to the skin effect of ferromagnetic materials, the penetration depth decreases with the increase of excitation coil frequency. Magnetic detection uses the magnetic field changes at the welds and defects of pipelines or the principle of magnetic flux leakage to detect and locate welds and defects [9], [20], [21], whereas, the detection accuracy is limited by the lift-off value; the lift-off value cannot be too large, and the sensor needs to be as close to the detection surface as possible. In [21], several investigations were carried out demonstrating the residual magnetic field variation and pattern can be used for assessing residual stress, applied stress and defects.

However, almost all the methods above focus on the defect detection of the weld, rather than the detection of the spiral-girth weld crosspoint. In addition, all the methods above need to be implemented with the cylindrical Pipeline Inspection Gauge (PIG) which is one of the most commonly used inline inspections (ILI). ILI can be carried out by installing various sensors on the PIG, such as magnetic flux leakage sensor, magnetometer, mileage wheel, ultrasonic tools, etc. While, PIGs are very large and bulky. Detection probe of the PIG based on the above method has to contact with the pipe wall. In order to obtain sufficient thrust from the pressure difference between the front and back of the PIG, the polyurethane leather cup of the PIG must have interference fit with the pipe wall [22]–[25]. Therefore, there is huge friction between the PIG and the pipe wall, which makes the PIG have a high risk of blockage.

Another type of pipeline inspection carrier is inner Spherical Detector (SD). The diameter of the SD is smaller than that of the pipeline, so the SD can quietly roll forward pushed by the flow in the pipeline. It is convenient to launch and retrieve the SD. The SD is not easy to get blocked and has high signal-to-noise ratio, so it is a promising new quasi real-time detection tool for pipelines [26]–[28]. The SD has been used in the detection of magnetic anomalies in pipelines, and can identify girth welds from the measured magnetic signals, but cannot identify spiral welds [28]. Afterwards, the structure of SD was optimized to achieve fixed-axis rotation by adding a tungsten disc as counterweight to improve the quality of detected signals [29], [30]. However, the existing SD is still unable to locate the crosspoint of spiral and girth welds. This is because the size of the SD and the number and layout of the magnetometers have not been specially optimized for spiral weld detection at present, and the SD can neither detect the weak magnetic anomaly caused by the spiral weld and nor judge the spiral direction.

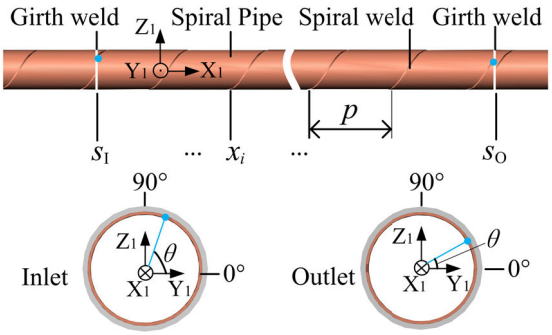

FIGURE 1. Schematic of detection principle of spiral-giirth weld crosspoint.

In order to locate the crosspoint of spiral and girth welds by using the SD, the following theoretical analysis and experimental research are carried out in this article: the principle of crosspoint localization is analyzed and the key technical points of magnetic detection of spiral welds are concluded; the sensor layout inside the SD is optimized to ensure that the magnetic signal of the spiral weld can be detected and the spiral direction can be identified; magnetic fields inside spiral steel pipe are measured by using the optimized SD to prove its feasibility of locating the spiral-girth weld crosspoints.

II. CROSSPOINT LOCALIZATION METHOD

A. LOCALIZATION PRINCIPLE

Definition and detection principle of the crosspoint of spiral and girth welds are shown in Figure 1. Pipeline coordinate system is denoted as $O_1{-}X_1Y_1Z_1$, and the position of the crosspoint of spiral and girth welds is defined as the rotation angle θ around the pipe axis $\mathbf{X_1}$ with $\mathbf{Y_1}$ as the rotation start.

The SD rolls forward on the pipe bottom and records internal magnetic fields and the acceleration of the rolling carrier. Girth welds and bottom spiral welds can be identified through magnetic features. By using the periodic acceleration signals to calculate the mileage of the SD, axial position s_I and s_O of the inlet and outlet girth welds as well as axial position x_i, $i = 1, 2, \ldots$ of each spiral weld can be determined in one section of spiral pipeline. As the angular position of each spiral weld at the pipe bottom is $\theta = 270°$, when taking the axial position x_i of each spiral weld at the bottom as a reference, the crosspoint location θ_{iI} of spiral-girth weld at the inlet can be expressed as:

$$\theta_{iI} = 270° \mp \left(\frac{s_I - x_i}{p} - \left\lfloor \frac{s_L - x_i}{p} \right\rfloor \right) \cdot 360°. \quad (1)$$

wherein, p is the spiral pitch; $\lfloor\ \rfloor$ means rounding down; $\mp$ takes $-/+$ when the spiral direction is levorotatory/dextrorotatory, which can be determined by the phase difference of side-by-side multi-channel magnetic signals. The number of identified spiral welds is denoted as n. Finally, the crosspoint location of the spiral-girth weld at the inlet is:

$$\theta_I = \frac{1}{n}\sum_{i=1}^{n}\theta_{iI}. \tag{2}$$

Similarly, the crosspoint location at the outlet is:

$$\theta_{iO} = 270°\pm\left(\frac{s_O - x_i}{p} - \left\lfloor\frac{s_O - x_i}{p}\right\rfloor\right)\cdot 360° \tag{3}$$

$$\theta_O = \frac{1}{n}\sum_{i=1}^{n}\theta_{iO}. \tag{4}$$

wherein $\pm$ takes $+/-$ when the spiral direction is levorotatory/dextrorotatory.

B. SENSOR LAYOUT

It can be concluded from the localization principle in Section 2.1 that there are two prerequisites for calculating the location of girth-spiral weld crosspoint: (1) identify at least one spiral weld using magnetic anomalies; (2) judge the spiral direction using multi-channel magnetic signals. The success of achieving these two key tasks depends on the advisable layout of the magnetometers. To optimize the magnetometer layout, magnetic field measurement experiments in a spiral steel pipe as shown in Figure 2 were carried out.

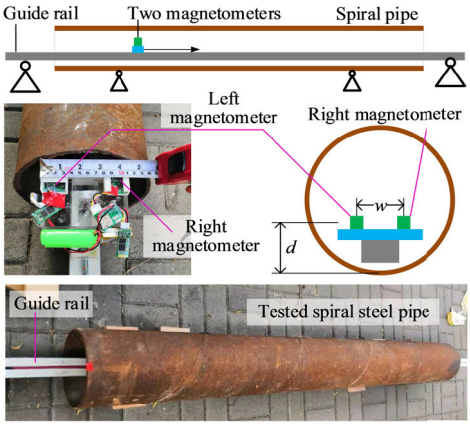

FIGURE 2. Experimental apparatus for testing sensor layout.

A non-magnetic straight aluminum guide rail passed through the spiral steel pipe, and two groups of wooden blocks with equal height were padded below two ends of the guide rail to ensure that the guide rail is parallel to the pipe axis. The tested spiral pipe is made of low carbon steel, and its outer diameter is 219mm, wall thickness is 6mm, and p is 425mm. Two magnetometers were fixed on a slider and the slider was pulled by a rope to slowly and uniformly slide on the guide rail from one end to the other end, and the magnetic signals were recorded at the same time. Connection line of the two magnetometers is parallel to the axis $\mathbf{Y_1}$, so that the two magnetometers can successively pass by a certain spiral weld one by one. The height of the guide rail was adjusted to observe the magnetic anomaly characteristics near the spiral weld with different lift-off values.

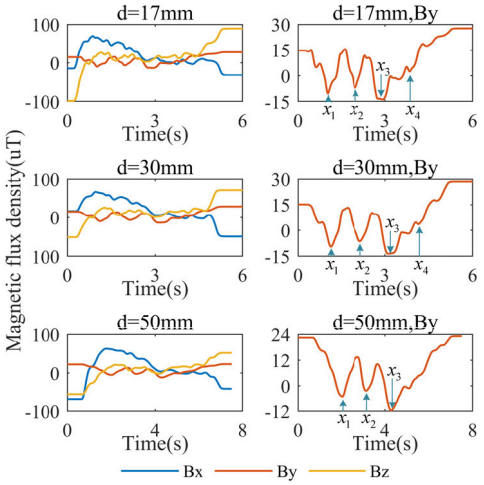

FIGURE 3. Schematic Magnetic fields in the spiral pipe on the measuring lines with different lift-off values.

The magnetic field distribution in the pipeline on the measuring line with lift-off value d of 17mm, 30mm, and 50mm is respectively shown in Figure 3. It can be seen that B_y component can clearly indicate the positions of the spiral welds. However, as the lift-off value increases, the amplitude of magnetic anomaly at the spiral weld gradually decreases. When d = 17mm, four spiral weld characteristic signals can be observed. Among them, the first peak-to-peak value is 25.6uT, and the fourth is 2.4uT. When d = 30mm, the four spiral weld characteristic signals can still be observed, but the amplitude is reduced. Among them, the first peak-to-peak value is 22.6uT, and that of the fourth is only 1.0uT. When d = 50mm, only three spiral weld characteristic signals can be observed, and the amplitude is further reduced. Among them, the peak-to-peak value of the first is 18.2uT, and that of the fourth cannot be observed. Therefore, in order to successfully detect spiral welds, on one hand, the SD's diameter should be reduced as much as possible so as to reduce the lift-off value; on the other hand, the magnetometer should be installed on the horizontal rotation axis that passes through the sphere center, so that the lift-off value is constant and equal to the radius of the SD. The diameter of a small SD is set to 60mm in the end.

Dual magnetometers deployed on the $\mathbf{Y_1}$ axis are used to determine the spiral direction. When the SD passes by a dextrorotatory spiral weld, the right magnetometer passes by the spiral weld first and the left magnetometer passes later, and vice versa. Space in the small SD is limited, so the interval distance w between the two magnetometers cannot be too large. w was set to 35mm and 70mm respectively to observe the magnetic characteristics near the weld of the

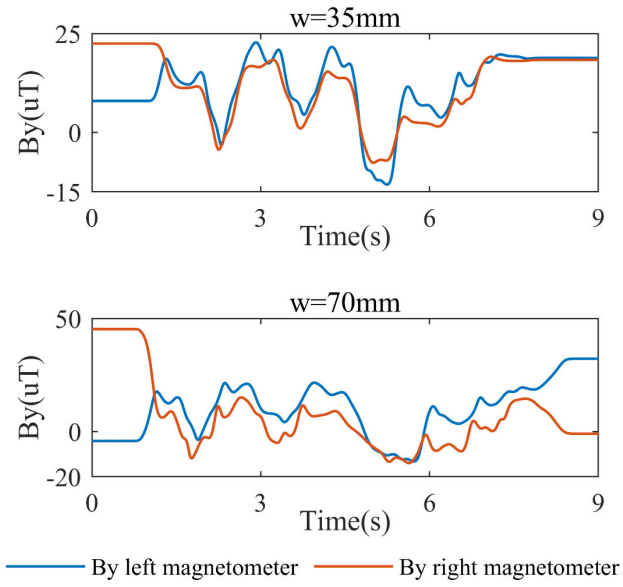

FIGURE 4. Magnetic signals of dual magnetometers.

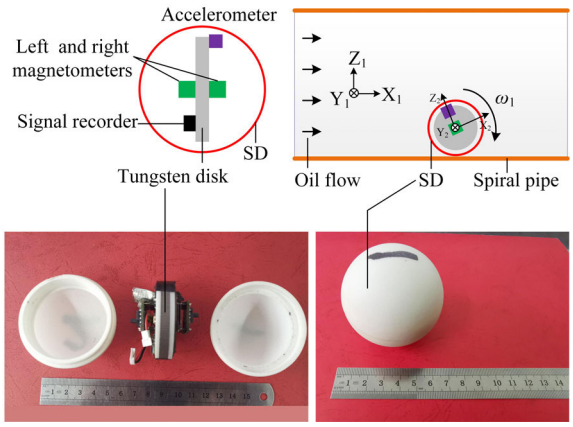

FIGURE 5. Device layout of and prototype of the small SD.

two channels, and the results are shown in Figure 4. It can be seen that the B_y component of the two magnetometers can both measure the concave magnetic characteristics of the spiral weld, and the magnetic valley of the right channel is ahead of that of the left channel, which is consistent with the actual situation. At the same time, as the distance between the two magnetometers decreases, the time difference between the left and right channel signals also decreases. When w is 35mm, the spiral direction can still be determined, and this distance can meet the layout requirements of the sensors in the small SD. Therefore, the interval distance w between the two magnetometers in the small SD is set to about 35 mm.

C. DESIGN OF SMALL SD

The small SD, which is used in liquid or gas pipelines, developed is shown in Figure 5. The SD's diameter is much smaller than the pipe diameter. A heavy tungsten disc is installed

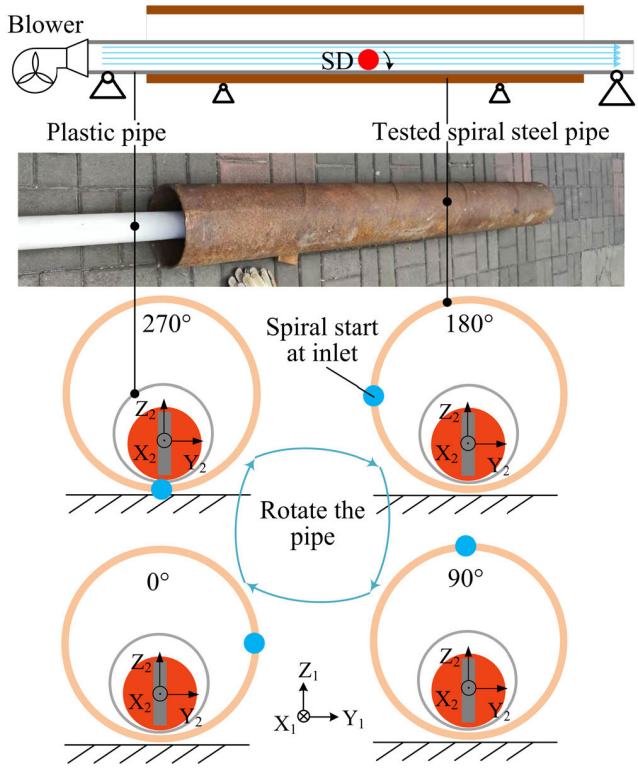

FIGURE 6. Experimental apparatus and process of locating the spiral-girth weld crosspoint using the small SD.

inside the SD, which concentrates 90% the mass of the SD, so that the rotational inertia of the SD around the axis $\mathbf{Y}_2$ is much larger than that around other axes, and the SD can stably roll around the axis of $\mathbf{Y}_2$, $\mathbf{Y}_2//\mathbf{Y}_1$. Dual magnetometers, accelerometer and signal recorder are fixed on the tungsten disc. The rotation axis of the accelerometer and magnetometers is also one of their sensitive axes $\mathbf{Y}_2$. Recorded B_y is analyzed to identify the spiral weld, and recorded a_x, a_z are used to calculate the SD's rolling mileage and then determine the positions of each spiral weld. Finally, according to the localization principle presented in Section 2.1, the position of the spiral-girth weld crosspoint is calculated.

III. EXPERIMENTS

A. CROSSPOINT LOCALIZATION EXEPERIMENT USING SMALL SD

Experimental apparatus and process for magnetically locating the spiral-girth weld crosspoint by using the small SD are shown in Figure 6. The tested spiral pipe is made of low carbon steel, and its outer diameter is 219mm, wall thickness is 6mm, and p is 425mm. The inner wall of the spiral pipe used in the experiment is not coated, and there are protrusions at the spiral weld. However, most of the spiral pipes used in the field are coated from the inside or have long-term accumulation of oil residue, so there is no protrusion at the spiral welds. Therefore, a plastic pipe is placed inside the spiral steel pipe to simulate the coating to provide the SD

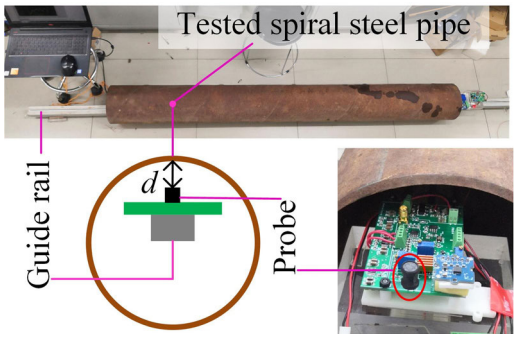

FIGURE 7. Experimental apparatus of eddy current testing method.

with a smooth contact surface similar to a field pipeline. An air pump was used to inject air flow into one end of the spiral pipe to push the SD to roll forward. The spiral steel pipe was rotated around its axis to obtain different spiral-girth weld crosspoints at the inlet and outlet. A total of four rotation tests were carried out. Each time the pipe rotation is accomplished, the SD still rolled forward on the bottom of the pipe. The small SD carries two magnetometers and an accelerometer. The two magnetometers are on the horizontal rotation axis passing through the center of the SD and are symmetrically located at two sides of the middle vertical plane. The accelerometer is installed at a distance from the axis of rotation.

B. CROSSPOINT LOCALIZATION EXEPERIMENT BY EDDY CURRENT INSPECTION

In order to further illustrate the effectiveness of the proposed method, eddy current testing experiments are carried out. As shown in Figure 7, the eddy current sensor is placed on a non-magnetic straight aluminum guide rail. And the guide rail passed through the spiral steel pipe, and two groups of wooden blocks with equal height were padded below two ends of the guide rail to ensure that the guide rail is parallel to the pipe axis. The lift-off values between the probe of the eddy current sensor and the inner wall is $d = 10$mm. During the test, pull the sensor slowly to ensure that the sensor passes through the pipe uniformly along the guide rail.

IV. RESULTS AND DISCUSSIONS

A. MAGNETIC SIGNALS AT SPIRAL WELDS MESURED BY THE SMALL SD

The magnetic fields inside the spiral pipe and carrier acceleration measured by the small SD in one of the experiments are shown in Figures 7 and 8. As can be seen from Figure 8, due to rolling, the measured B_x and B_z magnetic components look like sinusoidal signals with large fluctuations. Since the magnetic component B_y is collinear with the rolling axis of the SD, the fluctuation is very small, which can well indicate the lateral magnetic field distribution inside the spiral pipeline. B_y contains noticeable concave magnetic characteristics corresponding to the spiral weld. Because the small SD slightly

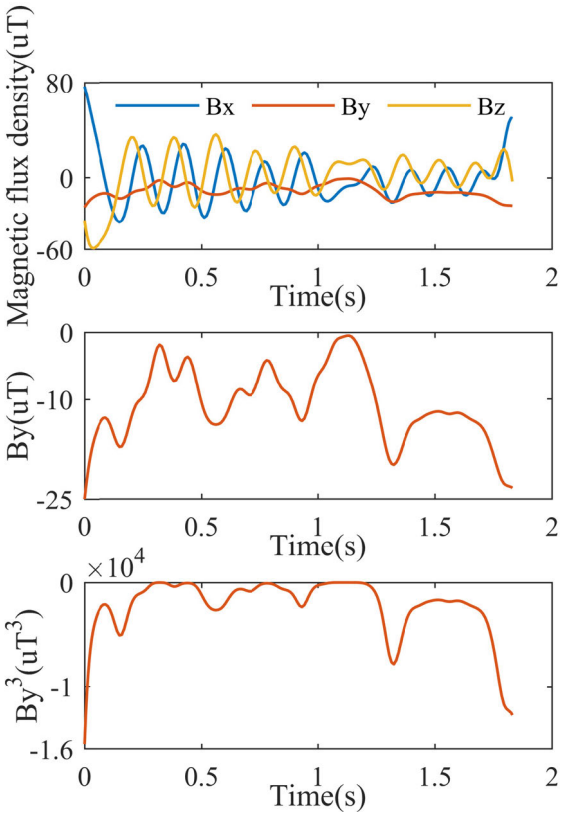

FIGURE 8. Internal magnetic fields of the spiral pipe measured by the small SD.

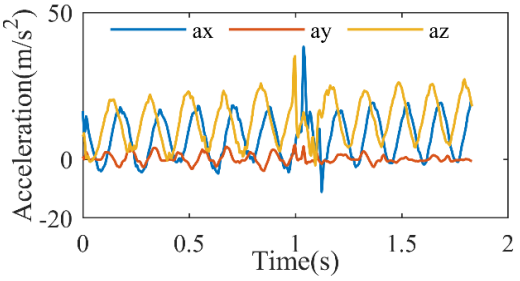

FIGURE 9. Acceleration signals measured by the small SD.

wobbles while rolling, there are some interference signals in B_y. Cubic operation of B_y can suppress the interference signal and enhance the spiral weld signal. In addition, the prior condition that the period of weld arising is fixed and known can be used to further eliminate the interference signal. For the previous larger SD, because its magnetometer fluctuates and is far from the bottom of the pipeline and none of its sensitive axes overlaps the horizontal axis to measure the lateral magnetic component, the spiral weld cannot be magnetically detected [28].

The acceleration signals recorded by the SD are shown in Figure 9. Amplitudes of a_x and a_z are much larger than that of a_y, indicating that the SD rotates around the axis $\mathbf{Y}_2$. The moving distance of the SD when rolling one circle is its perimeter, corresponding to a period of the acceleration

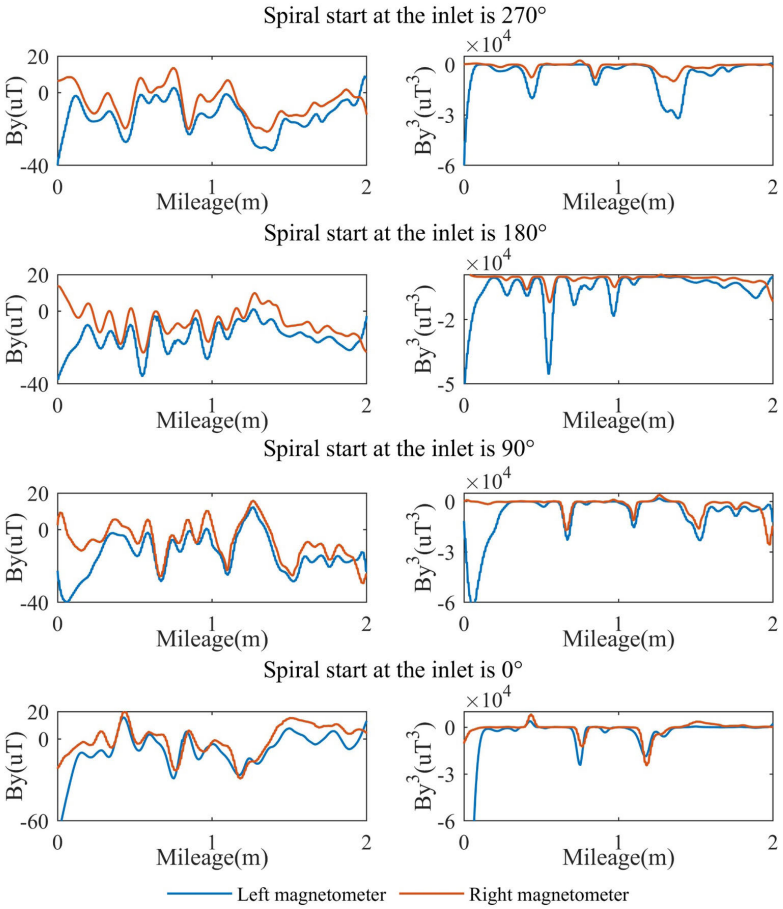

FIGURE 10. Measurement results of lateral magnetic fields inside the spiral steel pipe with different rotation angles.

signals. Mileage-time curve of the SD can be calculated using the acceleration signals. Since the time of magnetometer and accelerometer has been synchronized and aligned, the axial position of each spiral weld can be determined by comparing the mileage-time curve and the magnetic characteristic - time curve. Positioning results of each spiral weld are shown in Table 1. The average of measured pitch is 43.98cm, and the actual pitch of the pipeline is 42.5cm. The difference between the two is very small, only 1.48cm. Therefore, it is feasible to use the small SD to locate the spiral weld.

TABLE 1. Spiral weld position and spiral pitch measured by the small SD.

No.	x_1/cm	x_2/cm	x_3/cm	x_4/cm	x_5/cm	p/cm
1	16.0	58.4	100.9	148.0	--	44.0
2	--	58.4	103.7	147. 8	--	44.7
3	14.9	57.3	98.8	149.7	--	44.9
4	--	58.4	98.0	144.2	--	42.9
5	15.7	59.0	98.6	145.7	--	43.4

B. MEASUREMENT RESULTS OF THE CROSSPOINT OF SPIRAL AND GIRTH WELDS

The spiral steel pipe was rotated around its axis so that the starts of the spiral weld at the inlet are 270°, 180°, 90°, and 0°, respectively. The length of the tested spiral pipe is 2m and the pitch p is 425mm, so the start of the spiral weld at the outlet is always 105.9° larger than that at the inlet. For the four different rotations, the spiral-girth weld crosspoints at the inlet and outlet are known in the experiment. The small SD carrying two magnetometers was used to measure the internal magnetic component B_y. B_y and their cubic enhancement results are shown in Figure 10. It can be seen that after the cubic operation, the magnetic characteristics of the two channels at the spiral welds are noticeably concave. Combined with the acceleration signal, the measured positions of the spiral welds and the spiral-girth weld crosspoints at the inlet and outlet are shown in Table 2. It can be seen that the crosspoint localization errors are less than 30°, and their average is less than 20°, that is, no more than one hour's angle, whose accuracy is sufficient for excavation and maintenance in the field, because it will reduce the amount of excavation by nearly half.

C. COMPARISON WITH EDDY CURRENT TESTING

The results measured by eddy current testing method are shown in Figure 11. It can be seen that when the probe of

TABLE 2. Localization results by the SD of the spiral welds of the spiral pipe with different spiral starts and the crosspoint at the outlet.

Spiral start at		Channel	x_2/cm	x_3/cm	x_4/cm	θ_I/°	Error of θ_I/°	θ_O/°	Error of θ_O/°
inlet /°	outlet /°								
270	164.1	Left	43.4	84.9	128.8	257.4	-12.6	151.5	-12.6
		Right	44.3	85.6	131.6				
180	74.1	Left	54.6	97.1	--	164.6	-15.4	58.7	-15.4
		Right	55.5	97.6	--				
90	344.1	Left	65.9	109.8	152.2	60.8	-29.2	314.9	-29.2
		Right	66.8	110.2	153.3				
0	254.1	Left	75.3	117.9	--	348.4	-11.6	242.5	-11.6
		Right	76.4	118.4	--				

TABLE 3. Results of eddy current testing.

Spiral start at		x_1/cm	x_2/cm	x_3/cm	x_4/cm	x_5/cm	θ_I/°	Error of θ_I /°	θ_o /°	Error of θ_o /°
inlet /°	outlet /°									
105.9	0	18.8	60.0	104.1	149.0	191.0	104.2	-1.7	358.3	-1.7

the eddy current sensor passes through the spiral weld, the output voltage of the sensor would show noticeable concave characteristics. Combined with the acceleration signal, the measured positions of the spiral welds and the spiral-girth weld crosspoints at the inlet and outlet are shown in Table 3. It can be seen that the crosspoint localization error is 1.7° which is much smaller than the crosspoint error measured by the small SD. However, in order to ensure the detection accuracy of eddy current method, the sensor is required to move forward in the pipeline, that is to say, it must be mounted on the PIG. PIGs are very large and bulky which makes it have a higher risk of blockage than the small SD. Also, compared with the small SD, the manufacturing cost and detecting cost of PIGs are much higher. Therefore, the proposed method of locating the spiral-girth weld crosspoint based on the small SD is still of great significance.

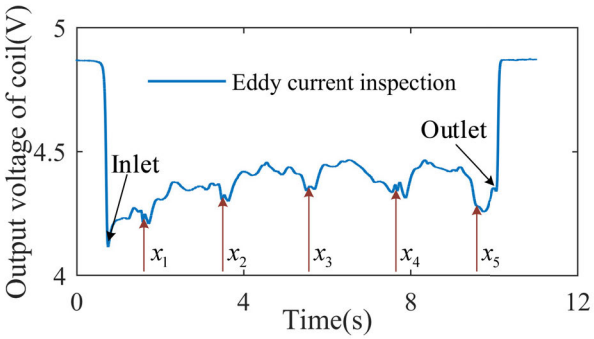

FIGURE 11. Result of eddy current testing.

D. FURTHER DISCUSSIONS

This article demonstrates a low cost, high efficiency method that can locate the crosspoint of spiral weld and girth weld based on the low cost small SD, and the accuracy is sufficient for excavation and maintenance in the field. This method also has some drawbacks that are not related to spiral weld localization, but related to pipeline defect detection. The SD can only detect the existence of spiral weld and girth weld, as well as large deformation and vibration of pipeline [28]–[30], but cannot detect weld defects and local corrosion defects of pipe wall, especially the upper side, left side, and right side which are far away from the SD. This is because that the diameter of the SD is smaller than the diameter of the pipe, the SD cannot contact the pipe wall. In addition, the SD is in the rotating state in the process of operation, and all the measured signals are modulated by rotation, which increases the difficulty of signal processing. However, PIGs do not have these problems.

This work also contributes to the body of knowledge. First, in the guide rail experiment, the magnetic anomaly of B_y component of spiral weld is more obvious than the other two components. The B_y component is parallel to the rolling axis of the SD, which enables the SD to be used to detect the existence of the spiral weld. Second, dual channels of magnetometers with a certain distance between the left and right are used for spiral weld detection. Under the guarantee of the measurement synchronization, when the SD rolls through the spiral weld, there will be a phase difference between the signals of the dual channels, which can be used to determine the direction of the spiral weld. At the same time, this phase

difference can also be used to eliminate the influence of interference peaks. For example, if there is a ''concave'' similar to the spiral weld characteristics in the measurement signal due to the rolling instability or the sudden change of the magnetic field in the pipe, it can be judged by comparing whether the ''concave'' of the dual channels has the phase difference, if so, it is the spiral weld, otherwise it is the interference peak. Third, placing a tungsten disk in the small SD can make the SD stably rotate. When the SD rolls around a fixed axis, the influence of the disturbance signal caused by unstable rolling can be reduced, and the difficulty of inversion of the SD attitude can also be relieved.

V. CONCLUSION

In this article, we propose a low-cost and high-efficiency method for locating the spiral-girth weld crosspoint based on the SD. Theoretical analysis and experiments demonstrate that crosspoint localization of the spiral and girth welds at the inlet and outlet of one section of spiral pipe can be achieved via detection and positioning of the spiral welds at the bottom and the spiral direction. Lateral magnetic fields near the spiral welds have noticeable concave characteristics and can be used to identify the spiral welds. In order to magnetically detect and locate the spiral welds, it is necessary to reduce the lift-off value of the magnetometer, so a small SD should be used. A smaller lift-off value can enhance the magnetic characteristics of the spiral welds. The spiral direction can be determined by the phase difference of the dual-channel magnetic signals. It is feasible to identify and locate the spiral welds and calculate the angular position of the crosspoint on the girth weld via measuring the interior magnetic fields and the carrier's acceleration by using the small SD.

There are still many areas worthy of further study in the future. We plan to change the size and shape of the heavy tungsten disk in the center of SD, explore the rolling characteristics of SD under different weights, and further improve the stability of fixed axis rolling. We intend to further enrich the functions of SD by adding relevant sensors that can detect the inclination of the pipeline to the SD, so that the SD can monitor and record changes in the inclination of the pipeline while rolling forward in the pipeline. The maximum localization error of the crosspoint is less than 30° and the average error is less than 20°, whose accuracy is sufficient for excavation and maintenance in the field. The localization error is still large. In this article, we suppress the interference signal and enhance the spiral weld signal using the cubic operation of By. Next, we plan to seek the appropriate neural network algorithm to enhance the spiral weld signal, eliminate the interference signal, and further improve the location accuracy.

REFERENCES

[1] Y. R. Feng, C. Y. Huo, L. K. Ji, and H. L. Li, ''Progress and prospect of research and application of high-grade pipeline steels & steel pipes in China,'' *Petroleum Sci. Bull.*, vol. 1, no. 1, pp. 143–153, 2016, doi: 10.3969/j.issn.2096-1693.2016.01.009.

[2] S. Al-Sulaiman, S. Safri, A. Salam, and C. Lee, ''Failure along spiral welds in gas pipeline,'' in *Proc. 11th Int. Pipeline Conf.*, Sep. 2016, Art. no. V001T03A001, doi: 10.1115/IPC2016-64030.

[3] Y. Luo, W. Jiang, Y. Wan, W. Woo, and S.-T. Tu, ''Effect of helix angle on residual stress in the spiral welded oil pipelines: Experimental and finite element modeling,'' *Int. J. Pressure Vessels Piping*, vol. 168, pp. 233–245, Dec. 2018, doi: 10.1016/j.ijpvp.2018.10.015.

[4] S. Akhshik, M. Behzad, and M. Rajabi, ''CFD–DEM approach to investigate the effect of drill pipe rotation on cuttings transport behavior,'' *J. Petroleum Sci. Eng.*, vol. 127, pp. 229–244, Mar. 2015, doi: 10.1016/j.petrol.2015.01.017.

[5] Y. Bian, C. Penniston, L. Collins, and R. Mackenzie, ''Evaluation of UOE and spiral-welded line pipe for strain based designs,'' in *Proc. 8th Int. Pipeline Conf.*, Jan. 2010, pp. 139–148, doi: 10.1115/IPC2010-31315.

[6] G. Chatzopoulou, G. C. Sarvanis, C. I. Papadaki, and S. A. Karamanos, ''The effect of spiral cold-bending manufacturing process on pipeline mechanical behavior,'' in *Proc. AMSE 11th Int. Pipeline Conf.*, Sep. 2016, pp. 1–10, doi: 10.1115/IPC2016-64143.

[7] X. Chen, H. Lu, G. Chen, and X. Wang, ''A comparison between fracture toughness at different locations of longitudinal submerged arc welded and spiral submerged arc welded joints of API X80 pipeline steels,'' *Eng. Fract. Mech.*, vol. 148, pp. 110–121, Nov. 2015, doi: 10.1016/j.engfracmech.2015.09.003.

[8] Q. Feng, Y.-H. Lin, F. Wang, and B. Li, ''Preliminary failure assessment for spiral welded defects of pipeline,'' in *Proc. 7th Int. Pipeline Conf.*, 2008, pp. 93–101, doi: 10.1115/IPC2008-64059.

[9] J. Chen, Q. Feng, F. Wang, H. Zhang, and H. Song, ''Research on burst tests of pipeline with spiral weld defects,'' in *Proc. Int. Pipeline Conf.*, Sep. 2012, pp. 53–60, doi: 10.1115/IPC2012-90089.

[10] M. S. Węglowski, S. Dymek, M. Kopyściański, J. Niagaj, J. Rykała, W. De Waele, and S. Hertelé, ''A comprehensive study on the microstructure and mechanical properties of arc girth welded joints of spiral welded high strength API X70 steel pipe,'' *Arch. Civil Mech. Eng.*, vol. 20, no. 1, Mar. 2020, doi: 10.1007/s43452-020-00018-0.

[11] Q. Zhang, Y. T. Dou, and Z. Zhang, ''Analysis of spiral weld cracking at pipeline,'' *Cailiao Rechuli Xuebao/Trans. Mater. Heat Treat.*, vol. 34, no. 7, pp. 112–117, 2013, doi: 10.13289/j.issn.1009-6264.2013.07.032.

[12] B. Taljat, T. Zacharia, X. L. Wang, and J. R. Keiser, ''Numerical analysis of residual stress distribution in tubes with spiral weld cladding,'' *Weld. J.*, vol. 77, no. 8, pp. 328–335, 1998.

[13] J. Zhang, G. Tian, A. Marindra, A. Sunny, and A. Zhao, ''A review of passive RFID tag antenna-based sensors and systems for structural health monitoring applications,'' *Sensors*, vol. 17, no. 2, p. 265, Jan. 2017, doi: 10.3390/s17020265.

[14] M. Michael and L. Simon, ''Special phased array applications for pipeline girth weld inspections,'' in *Proc. AMSE Pressure Vessels Piping Division Conf.*, 2006, pp. 1–9.

[15] C. H. Kim, J. Y. Kim, K. S. Song, and Y. H. Cha, ''Application of ultrasonic test system for test performance improvement of welding flaw,'' *Key Eng. Mater.*, vols. 321–323, pp. 1517–1521, Oct. 2006, doi: 10.4028/www.scientific.net/KEM.321-323.1517.

[16] R. Konrad, ''Eddy current testing in pipeline inspection,'' in *Oil Gas Pipelines*. Hoboken, NJ, USA: Wiley, 2015, pp. 537–544, doi: 10.1002/9781119019213.ch36.

[17] Z. Liang, W. Xuan, and T. Wang, ''Eddy current NDt for the cracks of girth welds of pipes based on 2D impedance characteristics,'' *Yi Qi Yi Biao Xue Bao/Chin. J. Sci. Instrum.*, vol. 38, no. 9, pp. 2138–2145, 2017, doi: 10.19650/j.cnki.cjsi.2017.09.006.

[18] S. L. Asher, A. Boenisch, and K. Reber, ''Development of a magnetic eddy current in-line inspection tool,'' in *Proc. AMSE 2016 11th Int. Pipeline Conf.*, Sep. 2016, pp. 1–7, doi: 10.1115/IPC2016-64369.

[19] L. Xie, B. Gao, G. Y. Tian, X. Xiao, S. Wu, Y. Yin, and D. Mao, ''Investigation of remote field eddy current defect detection for pipeline welds,'' in *Proc. IEEE Far East NDT New Technol. Appl. Forum (FENDT)*, Jul. 2018, pp. 41–137, doi: 10.1109/FENDT.2018.8681970.

[20] Q. Feng, J. Sutherland, B. Gu, Y. Wei, and C. Tao, ''Evolution of Triax magnetic flux leakage inspection for mitigation of spiral weld anomalies,'' in *Proc. 8th Int. Pipeline Conf.*, Jan. 2010, pp. 1–8, doi: 10.1115/IPC2010-31116.

[21] J. W. Wilson, G. Y. Tian, and S. Barrans, ''Residual magnetic field sensing for stress measurement,'' *Sens. Actuators A, Phys.*, vol. 135, no. 2, pp. 381–387, Apr. 2007, doi: 10.1016/j.sna.2006.08.010.

[22] L. J. Yang, B. Sun, and W. Guo, "Pipeline geographical coordinates Location algorithm based on positioning navigation technology," *J. Shenyang Univ. Technol.*, vol. 36, no. 1, pp. 66–71, 2014, doi: 10.7688/j.issn.1000-1646.2014.01.12.
[23] W. M. F. Al-Masri, M. F. Abdel-Hafez, and M. A. Jaradat, "Inertial navigation system of pipeline inspection gauge," *IEEE Trans. Control Syst. Technol.*, vol. 28, no. 2, pp. 609–616, Mar. 2020, doi: 10.1109/tcst.2018.2879628.
[24] F. R. Huang, L. Y. Sun, L. S. Guo, Y. Li, and F. Qian, "High-accuracy positioning method based on reverse navigation solution in pipeline detection," *J. Chin. Inertial Technol.*, vol. 26, no. 4, pp. 435–439, 2018, doi: 10.13695/j.cnki.12-1222/o3.2018.04.003.
[25] P. Zhang, C. M. Hancock, L. Lau, G. W. Roberts, and H. de Ligt, "Low-cost IMU and odometer tightly coupled integration with robust Kalman filter for underground 3-D pipeline mapping," *Measurement*, vol. 137, pp. 454–463, Apr. 2019, doi: 10.1016/j.measurement.2019.01.068.
[26] S. Guo, S. Chen, X. Huang, Y. Zhang, and S. Jin, "CFD and experimental investigations of drag force on spherical leak detector in pipe flows at high Reynolds number," *Comput. Model. Eng. Sci.*, vol. 101, no. 1, pp. 59–80, 2014, doi: 10.1016/j.physd.2014.04.003.
[27] X. J. Huang, S. L. Chen, T. S. Xu, Q. L. Ma, S. J. Jin, and G. S. Chirikjian, "A 3D localization approach for subsea pipelines using a spherical detector," *IEEE Sensors J.*, vol. 17, no. 6, pp. 36–1828, Mar. 2017, doi: 10.1109/JSEN.2016.2586998.
[28] Y. Zhang, X. Huang, S. Chen, S. Guo, and S. Jin, "Analyses of magnetic field in spiral steel pipe," *J. Magn. Magn. Mater.*, vol. 375, pp. 210–216, Feb. 2015, doi: 10.1016/j.jmmm.2014.10.006.
[29] G. Lin, Z. Zhoumo, H. Xinjing, L. Jian, and C. Shili, "Vibration detection of spanning subsea pipelines by using a spherical detector," *IEEE Access*, vol. 7, pp. 7001–7010, 2019, doi: 10.1109/ACCESS.2018.2890024.
[30] L. Jian, L. Mingze, H. Xinjing, F. Hao, and R. Xiaobo, "Lateral pipeline buckling detection via demagnetization and interior magnetic measurement," *IEEE Access*, vol. 8, pp. 7949–7957, 2020, doi: 10.1109/ACCESS.2020.2964766.

JIAN LI received the B.E., M.E., and Ph.D. degrees from TJU, in 1994, 1997, and 2000, respectively. He is currently a Professor with TJU. His research interests include pipeline leak detection and pipeline safety warning.

MINGZE LI received the B.S. degree from Tianjin University (TJU), in 2018, where he is currently pursuing the master's degree with the Instrument Science and Technology Department. His research interests include orientation and localization of pipelines.

XINJING HUANG received the B.S. and Ph.D. degrees from TJU, in 2010 and 2016, respectively. He is currently an Associate Professor with TJU. His research interests include structural health monitoring and damage detection for infrastructure.

FENG HAO, photograph and biography not available at the time of publication.

XIAOBO RUI, photograph and biography not available at the time of publication.

YU ZHANG, photograph and biography not available at the time of publication.